Desalination and Water Treatment
www.deswater.com

doi: 10.5004/dwt.2021.27491

231 (2021) 205–216
August

Visible light irradiated photocatalytic activity of copper substituted $CoMn_2O_4$ nanoparticles

Nagina Bashir[a], Humera Sabeeh[a], Sonia Zulfiqar[b], Anwar Ali Shad[c], Muhammad Suleman[c], Philips O Agboola[d], Imran Shakir[e], Najeeb Faud Al-Khalli[f], Muhammad Farooq Warsi[a,*]

[a]*Institute of Chemistry, Baghdad-ul-Jadeed Campus, The Islamia University of Bahawalpur, Bahawalpur-63100, Pakistan, emails: Farooq.warsi@iub.edu.pk (M.F. Warsi), naginabashir34@gmail.com (N. Bashir), humera.sabeeh1992@gmail.com (H. Sabeeh)*
[b]*Department of Chemistry, School of Sciences & Engineering, The American University in Cairo, New Cairo 11835, Egypt, email: sonia.zulfiqar@aucegypt.edu*
[c]*Department of Agriculture Chemistry, Agriculture University Peshawar, KPK, Pakistan, emails: anwaralishad@aup.edu.pk (A.A. Shad), suleman@aup.edu.pk (M. Suleman)*
[d]*College of Engineering, Al-Muzahmia Branch, King Saud University, P.O. Box: 800, Riyadh 11421, Saudi Arabia, email: paboola@ksu.edu.sa*
[e]*Sustainable Energy Technologies (SET) Center, College of Engineering, King Saud University, P.O. Box: 800, Riyadh 11421, Saudi Arabia, email: mshakir@ksu.edu.sa*
[f]*Department of Electrical Engineering, King Saud University, P.O. Box: 800, Riyadh 11421, Saudi Arabia, email: najeebalkhalli786@gmail.com*

Received 24 February 2021; Accepted 1 June 2021

ABSTRACT

In the current investigation, copper substituted cobalt manganese spinel oxide ($Cu_xCo_{1-x}Mn_2O_4$) photocatalyst was prepared via the co-precipitation method. The synthesized nanoparticles were characterized by X-ray diffraction, field emission scanning electron microscopy, and Fourier-transform infrared spectroscopy. The prepared $Cu_{0.2}Co_{1-0.2}Mn_2O_4$ nanoparticle exhibited excellent photocatalytic activity for degradation of typical organic-based dye Methylene blue (MB). Furthermore, the comparative study of pure $CoMn_2O_4$ and Cu-substituted $CoMn_2O_4$ nanoparticles (NPs) towards the photocatalytic performance was also conducted. As compared to the $CoMn_2O_4$ nanoparticles, the $Cu_xCo_{1-x}Mn_2O_4$ nanoparticles exhibited excellent photocatalytic capability for the degradation of MB dye. After 80 min of visible light irradiation, the decomposition of MB by $Cu_xCo_{1-x}Mn_2O_4$ nanoparticles was higher as compared to degradation MB dye in the presence of copper substituted $CoMn_2O_4$ NPs. Copper substituted cobalt manganese oxide nano-photocatalyst was also used for comparative study. The $Cu_{0.2}Co_{(1-0.2)}Mn_2O_4$ showed excellent (~86%) photocatalytic performance in contrast with $Cu_0CoMn_{(1-0)}O_4$ (22%), $Cu_{0.5}Co_{(1-0.5)}Mn_2O_4$ (57), $Cu_{0.1}Co_{(1-0.1)}Mn_2O_4$ (60%), $Cu_{0.15}Co_{(1-0.15)}Mn_2O_4$ (73%) for the degradation of MB in visible light irradiation. The enhanced photocatalytic activity is mainly attributed to the optimized bandgap, which might have developed by the inclusion of copper ions into the $CoMn_2O_4$ spinel oxide. The copper substitution not only contributed to the inhibition of photo-induced electron–hole pairs but also assisted a great redox capability. $Cu_xCo_{1-x}Mn_2O_4$ photocatalyst holds great potential for massive pollutant treatment due to the superb photocatalytic performance for organic pollutants.

Keywords: Nanoparticles; Spinel oxide; X-ray diffraction; Photocatalysis

* Corresponding author.

1. Introduction

Increased utilization of fossil fuels involved the rapid depletion of energy resources as well as raised environmental safety concerns [1]. Environmental pollution is the most debatable subject for the last few decades. Water (ground and surface) being an indispensable entity to living organisms is always at risk due to commercialization and economic growth. To control pollution, the removal of pollutants from water such as hydrocarbons, organic dyes, and pesticides is of great interest [2,3]. Typically the organic dyes and pesticides due to their large applications and persistence are being extensively studied [4,5]. Nevertheless, pollutants are of great risk to environmental safety, their remediation and mitigation demand more resources and energy [6]. The waste of simulated dye is the main derivatives of organic hydrocarbons which are utilized as a pigment in large quantities in different industries such as textiles, cosmetics, food, paper, and medicines [7]. The effluents of industries are contaminated with organic dyes, hence can pose a potential threat to aquatic organisms [8]. The elimination or remediation of these pollutants from effluents is, therefore, an important strategy to reduce the hazards associated with these chemicals [9]. Different approaches such as physical adsorption, oxidation, and microbial degradation are being studied and investigated. Photocatalysis being a cheap, easy and environmentally friendly technique has been extensively studied so far for the mitigation of organic toxins. If there is a suitable photocatalyst, sunlight or UV light are successfully applied to completely mineralized or convert them into non-toxic compounds [10]. This is a green method for the rapid deterioration of these dyes which results in the conversion of toxic compounds into non-toxic compounds [11]. Developing materials and technologies for a sustainable environment, aiming at removing dye effluents effectively, has been the consensus of many scientists, industrialists, and governments [12].

In the past few years, the formation of metal-based semiconductors is of much attention for the study of photocatalysis [13,14]. Nanostructured materials have been widely used because of their significant magnetic, electrical, optical, and chemical characteristics. These nanostructured materials are inaugurated to be regulated by their size, shape as well as surface by volume ratio between all [15]. Due to their remarkable properties, these materials are widely used for the formation of many advanced materials having well-defined structures [16]. Consequently, much more interest has been provided to the formation of carbon-based nanomaterials, transition metals and metal oxides which are used as a catalyst. In the last few years, oxides of metals have been detailed studied because they are highly reactive as well as have long-term chemical and thermal stability, moreover, recycling and restoration properties make them affordable catalysts. For the various organic catalytic reactions, the spinel-type metal-based oxides (AB_2O_4) are considered as a catalyst [17]. However, composites of manganese oxide have quite strong adsorption capabilities [18]. Besides, $CoMn_2O_4$ spinel nanostructure has attracted the researcher's consideration due to its cost-friendly production, environmentally friendly, stability, and broad applications, for example, photocatalysis and electro-catalysis [19].

However, the use of $CoMn_2O_4$ as a photocatalyst is restricted because of their strong electron-hole pair recombination ability and very low charge separation capacity. Such behavior of $CoMn_2O_4$ photocatalyst devalues its significance in photocatalysis [3]. To reduce the recombination of charges, these nanostructured are used to prepare their composites which are generally used instead of these, as a result, the photo-induced electron can travel from one material to another material because of appropriate matching of energy band at the surface [20]. These features are further increased through the usage of divalent MIs, for example, Ni^{2+}, Co^{2+}, Cu^{2+} as a dopant. Between the all divalent metal ions (MIs), the Cu^{2+} peculiarly exhibited remarkable catalytic characteristics with $CoMn_2O_4$ NPs. Omidvar et al. [21] prepared a GO/Fe_3O_4/Pd nanocomposites via a simple method and its catalytic activity has been tested for the reduction of 4-nitrophenol, Methyl orange, Methylene blue (MB), and Congo red. The transmission electron microscopy (TEM), X-ray diffraction (XRD), scanning electron microscopy (SEM), energy-dispersive X-ray spectroscopy (EDS), and Fourier-transform infrared (FT-IR) spectroscopic analyses confirmed the formation of GO/Fe_3O_4/Pd nanocomposite. Nasrollahzadeh et al. [22] reported the advanced carbonaceous nanomaterials and methodologies for photocatalysis purpose. The prepared catalyst was deployed for the elimination of contaminants and ionic metals in aqueous media, and as a novel nanosorbent for wastewater, drinking, and groundwater treatment. Naghdi et al. [23] synthesized the Cu/GO/MnO_2 nanocomposite through the reduction of Cu^{2+} ions to Cu(0) in the presence of *Cuscuta reflexa* leaf extract and immobilization of CuNPs on the GO/MnO_2 surface under organic solvent-free conditions. The GO/MnO_2 and Cu/GO/MnO_2 nanocomposites were fully characterized by various techniques such as FT-IR, XRD, field emission scanning electron microscopy (FE-SEM), TEM, high-resolution transmission electron microscopy, EDS, Brunauer–Emmett–Teller, thermogravimetric analysis, vibrating sample magnetometer and elemental mapping. Nasrollahzadeh et al. [24,25] prepared the Pd nanoparticles (NPs)/reduced graphene oxide (rGO) nanocomposite in a one-pot process by using *Euphorbia stenoclada* extract as antioxidant media in the absence of any surfactant, dangerous reactants, or using external energy input. Catalytic potential of the fabricated Pd-rGO nanocomposite was examined for the degradation of environmental contaminants including Cr(VI), 4-nitrophenol, Congo red, Methylene blue (MB) and Methyl orange. Nasrollahzadeh et al. [26] discussed that green-synthesized and biogenic nanocatalysts and nanomaterials can cost-effectively and proficiently eliminate the inorganic, organic, pharmaceutical, and heavy metal pollutants from the aqueous streams. Nasrollahzadeh et al. [27,28] reported the natural biopolymers, polymeric organic molecules produced by living organisms or renewable resources, are considered greener, sustainable, and eco-friendly materials.

Among many organic pollutants, the typical organic dye Methylene blue (MB) has been used to study the photocatalytic performance of synthesized nanoparticles under visible light. The processes included in photocatalysis have been explained through the degradation of the Methylene blue mechanism.

Here in this paper, the Cu-substituted $CoMn_2O_4$ nanoparticles as a photocatalyst are used to study the

effect of various reaction parameters, for example, temperature, pH, and amount of photocatalyst on photocatalytic efficiency in a detailed manner. The results indicate that Cu substituted $CoMn_2O_4$ nanoparticles photocatalyst are a promising candidate in photocatalytic applications under visible light.

2. Experimental section

2.1. Materials

The list of materials that are used for the preparation of $CoMn_2O_4$ and Cu-substituted $CoMn_2O_4$ is listed below in Table 1.

2.2. Synthesis of $CoMn_2O_4$ nanoparticles

A co-precipitation strategy was utilized to fabricate the $CoMn_2O_4$ nanoparticles. Manganese acetate and cobalt chloride aqueous solutions of equal molarity (0.1 M) were prepared in (1:1) water–ethanol mixture and after that solutions were mixed to get a clear reaction mixture. Ti thus reaction mixture, oxalic acid (0.5 g) was added with consistent stirring. After the dissolution of oxalic acid, sodium hydroxide (10 mL of 1 M) was added and stirred again for 12 h at 80°C. The addition of sodium hydroxide turned the color of the solution into dark green. After the completion of the reaction, the precipitates were washed with water and ethanol to elute the unreacted precursors. The precipitates were dried in an oven at 60°C for almost 24 h and calcined at 450°C for 2 h. The calcined samples were packed and stored for further structural, spectral and photocatalytic properties studies [29,30]. The entire synthetic experimental procedure is depicted in Fig. 1.

Table 1
List of chemicals used in the synthesis of pure $CoMn_2O_4$ and Cu-substituted $CoMn_2O_4$ nanoparticles

Sr. No.	Chemical name	Molecular formula
1.	Manganese acetate	$Mn(CH_3COOH)_2$
2.	Cobalt chloride	$CoCl_2{\cdot}6H_2O$
3.	Oxalic acid	$C_2H_2O_4$
4.	Sodium hydroxide	NaOH
5.	Ethanol	C_2H_5OH
6.	Copper acetate	$CuCl_2$
7.	Distilled water	H_2O

2.3. Synthesis of Cu-substituted $CoMn_2O_4$ nanoparticles

The above-synthesized $CoMn_2O_4$ nanoparticle was substituted with copper in different weight % ratios which are shown in Table 2.

2.4. Characterization

XRD technique was employed to investigate the crystal structure and phase determination of the above-prepared spinel oxide nanoparticles. ZEISS LEO SUPRA 55 was used for morphological analysis. Fourier-transform infrared spectroscopy was performed for structure interpretation.

Table 2
Composition of copper substituted $CoMn_2O_4$ nanoparticles

Sr. No.	Composition	Cu (weight%), X = Cu
1.	$CoMn_2O_4$	X = 0, (0%)
2.	$Cu_{0.05}Co_{(1-0.05)}Mn_2O_4$	X = 0.05, (5%)
3.	$Cu_{0.1}Co_{(1-0.1)}Mn_2O_4$	X = 0.1, (10%)
4.	$Cu_{0.15}Co_{(1-0.15)}Mn_2O_4$	X = 0.15, (15%)
5.	$Cu_{0.2}Co_{(1-0.2)}Mn_2O_4$	X = 0.2, (20%)

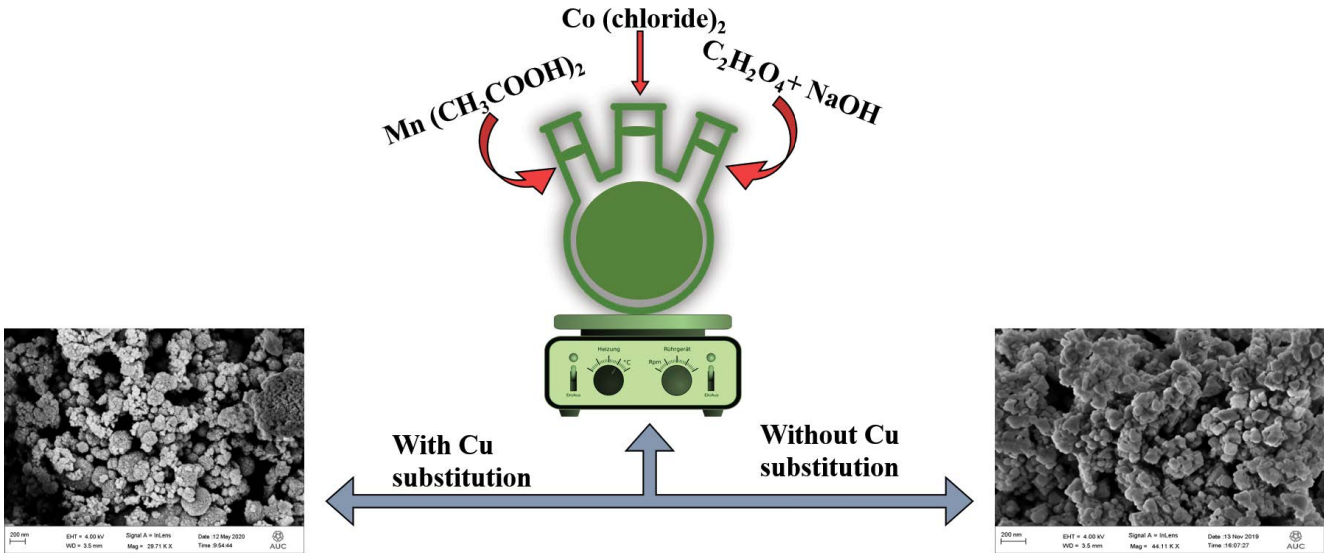

Fig. 1. Synthesize Cu-substituted $CoMn_2O_4$ and unsubstituted $CoMn_2O_4$ nanoparticles.

Optical characterization of the samples was done by UV-Vis dual-beam spectrophotometer.

2.5. Photocatalytic experiment

For the study of photocatalytic activity of pure $CoMn_2O_4$ and Cu-substituted $CoMn_2O_4$ nanoparticles, Methylene blue (MB) was used for oxidative photodegradation. In this experiment, solar light was used as an energy source for the photocatalysis experiment. In the procedure of photocatalysis, the powdered sample (5 mg) was added in Methylene blue (50 mL of 5 ppm) solution. The solutions were prepared in distilled water. In order to produce strong adsorption-desorption equilibria between the dye solution and sample used as a photocatalyst, continuously stirring is required in the dark for 30 min. To eliminate all the photocatalyst particles, the 5 mL of sample was centrifuged at pre-determined intervals of visible light. By applying the same photocatalytic conditions, various factors such as, amount of catalyst that has a great influence on the photocatalyst activity and rate of degradation of dye were studied in detail. The % removal of MB dye was calculated by the given equation:

$$X(\%) = 1 - \frac{C_t}{C_0} \quad (1)$$

where C_0 is the initial concentration and C_t is the concentration at any time 't' of MB dye.

3. Results and discussion

3.1. XRD analysis

XRD diffraction studies were used to examine the crystalline structure of pure and Cu-substituted $CoMn_2O_4$ nanoparticles. The recorded XRD patterns are given in Fig. 2. From Fig. 2 it is clear that all the prepared samples have the almost same XRD patterns. The formation of spinel structure has good consistency with JCPDS card no. 77-0471 [31,32]. As it is clear from the figure that there is no formation of secondary phase and no impurity in the XRD pattern, therefore the prepared samples have high crystallinity. Typical 2θ values with their corresponding hkl values are given in Table 3.

After the substitution of copper in the $CoMn_2O_4$ crystal lattice, the extra peaks in the diffraction patterns of the substituted samples have appeared. These peaks are given in Table 3. These peaks have good consistency with the development of the CuO pattern of JCPDS card no. 05-0661. The three peaks at angle 38.7° and 49° and 68.9° corresponds to CuO in the remaining four substituent particles which indicated the substitution of desired copper in $CoMn_2O_4$ nanoparticles along with the appearance of the secondary phase of copper oxide.

The crystallite size of $CoMn_2O_4$ nanoparticle was determined by the Debye–Scherrer formula,

$$D = \frac{K\lambda}{\beta\cos\theta} \quad (2)$$

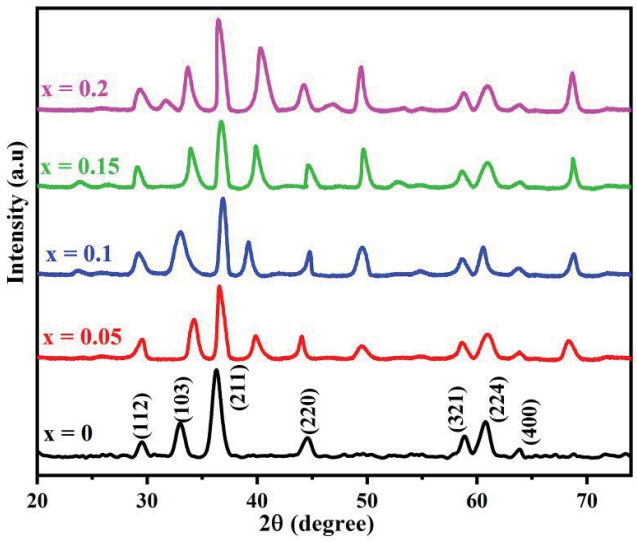

Fig. 2. XRD patterns of pure spinel and Cu-substituted spinel oxide nanoparticle $x = 0$ corresponds to $CoMn_2O_4$; $x = 0.05$ corresponds to $Cu_{0.05}Co_{(1-0.05)}Mn_2O_4$; $x = 0.1$ corresponds to $Cu_{0.1}Co_{(1-0.1)}Mn_2O_4$; $x = 0.15$ corresponds to $Cu_{0.15}Co_{(1-0.15)}Mn_2O_4$; $x = 0.2$ corresponds to $Cu_{0.2}Co_{(1-0.2)}Mn_2O_4$ NPs.

Table 3
The 2θ values for corresponding peaks appeared in XRD spectra of pure $CoMn_2O_4$ and Cu-substituted $CoMn_2O_4$ nanoparticles

	2θ	hkl
$CoMn_2O_4$	29.3°	(112)
	33.5°	(103)
	36.27°	(211)
	44.25°	(220)
	58.36°	(321)
	60.8°	(224)
	64.3°	(400)
$Cu_{0.2}CoMn_{(1-0.2)}O_4$	38.7°	(111)
	48°	(–202)
	68.1°	(220)

where K is the constant (0.99), λ represents the wavelength of the X-rays beam used in X-ray diffractometer, β is full-width at half maximum and θ is Bragg's diffraction angle.

3.2. FE-SEM analysis

The morphological study of the above-prepared nanoparticles was performed through a field emission scanning electron microscope. The room temperature morphological analysis was carried out for pure spinel oxide nanoparticles ($CoMn_2O_4$) and one typical sample from Cr-substituted $CoMn_2O_4$ nanoparticles. Fig. 3a shows the morphological structure of pure $CoMn_2O_4$ nanoparticles and Fig. 3b shows the Cu-substituted $CoMn_2O_4$. It is confirmed from the SEM analysis that the prepared nanoparticles have some agglomeration. The agglomeration might be due to multiple reasons. For example, the most common reason is

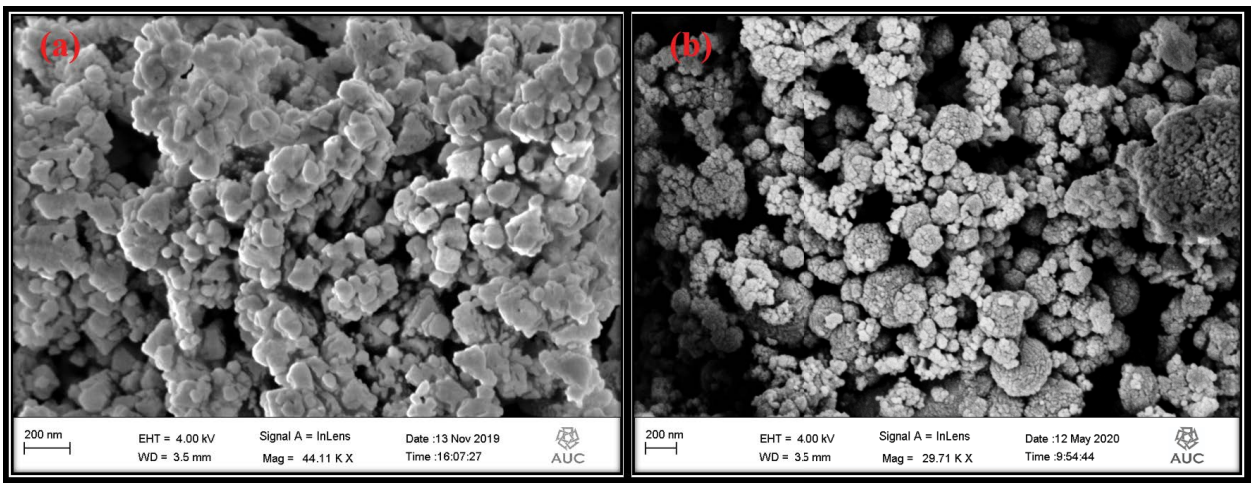

Fig. 3. FE-SEM illustrations of (a) $CoMn_2O_4$ NPs and (b) $Cu_{0.2}Co_{(1-0.2)}Mn_2O_4$.

that this the inherent property of metal oxide particles, that they can aggregate easily if they were not handled properly. The second reason may be the inappropriate handling during sample preparation for SEM analysis. On average the particle size was found <50 nm in both images.

3.3. FT-IR analysis

FT-IR spectra of pure $CoMn_2O_4$ and substituted $CoMn_2O_4$ are shown in Fig. 4. There are several peaks observed in the spectra. All these peaks have been explained as follows. The peak observed at 3,410 cm^{-1} corresponded to the vibration band of –OH. The absorption peaks appeared at 1,037 and 1,620 cm^{-1} corresponded to C–O–C and C=C respectively. The vibration bands near at 2,930 and 2,840 cm^{-1} were for C–H bond represented the three types of functional groups having oxygen, –OH, CH–O–CH and C=O. The adsorption peaks under 1,000 cm^{-1} mostly common in all manganites. The two main absorption peaks were shown at 500 and 612 cm^{-1}. These peaks are due to the bending vibration of manganese oxide (MnO) and cobalt oxide (CoO) of spinel $CoMn_2O_4$ [33]. All these vibration bands were identified in the spectrum for $CoMn_2O_4$ as well as the typical stretched vibrational absorption peaks observed at 2,933 and 1,030 cm^{-1} belong to the symmetric and asymmetric stretching vibration of the O–H and Cu–O bond corresponds to all Cu-substituted $CoMn_2O_4$ nanoparticles [34].

3.4. Current-voltage measurements

The current-voltage measurements for Cu substituted spinel oxide was carried out by using a Kiethely source meter. Fig. 5 represents the I-V curves for all five samples of different compositions of as-prepared spinel oxide nanoparticles. From the figure, it was seen that the I-V profile of pure $CoMn_2O_4$ nanoparticles is tilted and less linear. The linear behavior was observed to increase with increase Cu-contents in prepared spinel oxide nanoparticles. This linear behavior indicated the increased conductivity of prepared spinel oxide nanoparticles. Thus, it has been concluded that the substitution of Copper increased the conductivity of $CoMn_2O_4$ spinel oxides.

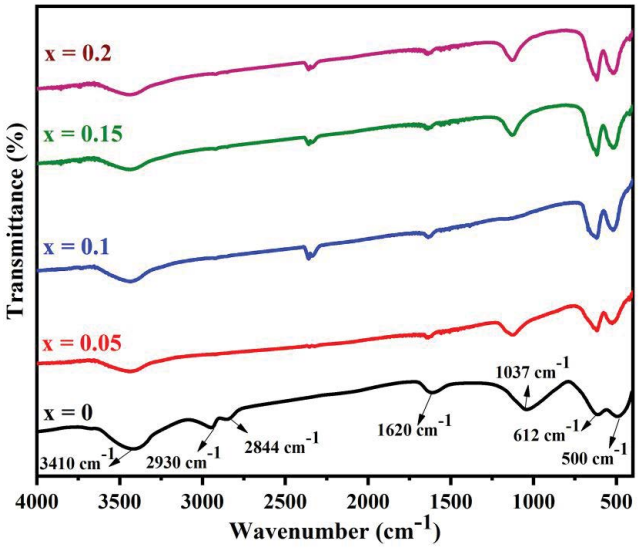

Fig. 4. FT-IR spectra of $x = 0$ corresponds to $CoMn_2O_4$; $x = 0.05$ corresponds to $Cu_{0.05}Co_{(1-0.05)}Mn_2O_4$; $x = 0.1$ corresponds to $Cu_{0.1}Co_{(1-0.1)}Mn_2O_4$; $x = 0.15$ corresponds to $Cu_{0.15}Co_{(1-0.15)}Mn_2O_4$; $x = 0.2$ corresponds to $Cu_{0.2}Co_{(1-0.2)}Mn_2O_4$ NPs.

The electrical conductivity (σ) values for all samples were calculated by using the following common mathematical equation.

$$\sigma = \frac{w}{RA} \tag{3}$$

where 'w' is the width of pellet, R for the resistance, and A for the area of samples pellets. The conventional digital screw gauge was used to determine the width 'w' and area 'A' of prepared pellets.

3.5. UV-Visible analysis

The UV-visible spectra of $CoMn_2O_4$ nanoparticles along with its derivative prepared by Cu-substitution

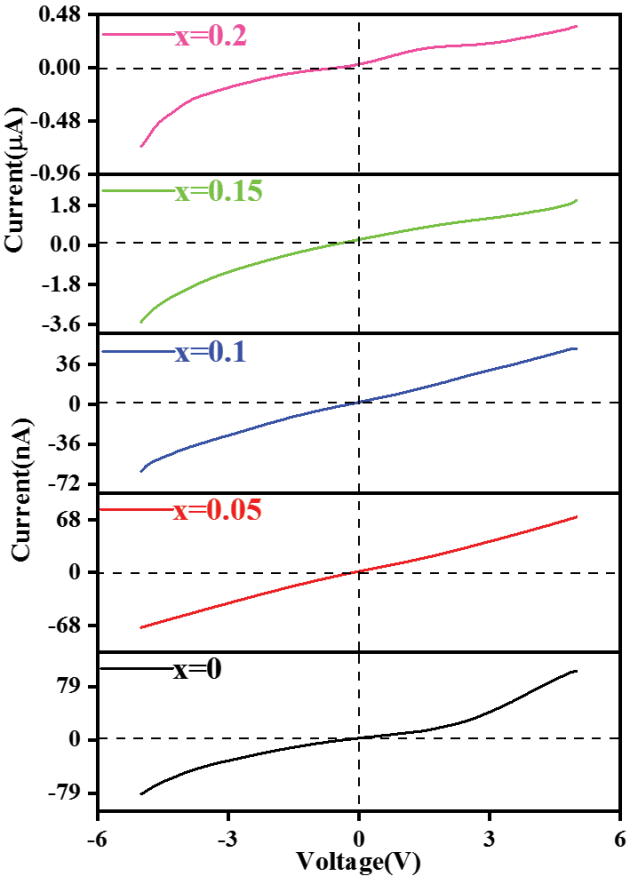

Fig. 5. I-V profiles of $x = 0$ corresponds to $CoMn_2O_4$; $x = 0.05$ corresponds to $Cu_{0.05}Co_{(1-0.05)}Mn_2O_4$; $x = 0.1$ corresponds to $Cu_{0.1}Co_{(1-0.1)}Mn_2O_4$; $x = 0.15$ corresponds to $Cu_{0.15}Co_{(1-0.15)}Mn_2O_4$; $x = 0.2$ corresponds to $Cu_{0.2}Co_{(1-0.2)}Mn_2O_4$ NPs.

with different percentages were recorded in the UV-Visible range of 200–800 nm. The information of transformation of negatively charged electrons inside the atom and molecules can be studied through UV-Vis spectra. Various parameters are used to investigate the photocatalysis of the materials. These parameters are the crystallinity of material, its absorption capability, attachment of the dye onto the surface of crystal structure, and reunion of charge carriers. The UV-Visible spectrum of $CoMn_2O_4$ spinel nanoparticles has been clearly shown in Fig. 6a. This spectrum contains the wide peak that appeared at 561 nm [35]. The UV-Vis absorption spectra of copper substituted cobalt manganese oxide ($CoMn_2O_4$) with different ratios are displayed in Figs. 6b–e. The sharp band at 425 nm and 220 nm for CuO confirmed that the pure $CoMn_2O_4$ and Cu-substituted $CoMn_2O_4$ are highly efficient to absorb in ultraviolet and visible regions.

The optical bandgap energy highly depends on the size, dimensions, and shape of the prepared particles. Bandgap energy of the prepared nanoparticles was evaluated from the Tauc Eq. (4) [36].

$$(\alpha h\nu)^n = A(h\nu - E_g) \quad (4)$$

In this equation α represents the absorption coefficient, h is for plank's constant, ν for light energy, A is the characteristic constant of the particle, E_g represents the bandgap energy and n is a constant which depends upon the nature of the transition of electrons. It can be ½ for indirect and 2 for direct transition. By plotting a graph between $(\alpha h\nu)^2$ on the y-axis and $h\nu$ on the x-axis, the bandgap of a particle can be calculated. The straight line of the resulted curve is extrapolated to the x-axis, to obtain the value of band gap energy in electron-volts (eV) [37,38]. Figs. 7a and 6b–e represent the Tauc plots of $Cu_0Co_{(1-0)}Mn_2O_4$, $Cu_{0.05}Co_{(1-0.05)}Mn_2O_4$, $Cu_{0.1}Co_{(1-0.1)}Mn_2O_4$, $Cu_{0.15}Co_{(1-0.15)}Mn_2O_4$ and $Cu_{0.2}Co_{(1-0.2)}Mn_2O_4$ respectively. The calculated values of the bandgap for $x = 0$, $x = 0.05$, $x = 0.1$, $x = 0.15$ and $x = 0.2$ were 1.540, 1.538, 1.536, 1.531 and 1.529 eV respectively. $Cu_{0.2}Co_{(1-0.2)}Mn_2O_4$ has a broad value of bandgap energy than all other synthesized Cu-substituted $CoMn_2O_4$ spinel oxides.

3.5.1. Mechanism of photocatalytic degradation

In the presence of sunlight, the photocatalytic reactions are treated to perform redox reactions. The reason for taking place the oxidation–reduction reactions is to expose the photocatalyst to sunlight. After that, conduction band holes are generated due to the excitation of valance electrons and produced by electron–hole pairs. The redox reaction took place due to these valance electrons. In photocatalysis when aqueous medium than H_2O is used and then hydroxyl (OH^-) react with hole and form $OH^\bullet$ radical which plays the role of primary oxidant. The electron–hole pair is developed when Cu-substituted $CoMn_2O_4$ NPs are exposed to visible light. Besides these, the electron–hole pairs recombine when we used unsubstituted $CoMn_2O_4$ NPs, while in Cu-substituted $CoMn_2O_4$ NPs, there electron-hole pair recombination was decreased. The reaction of electrons present in the conduction band with oxygen gives $O_2^{\bullet-}$. The MB dye is degraded by these $O_2^{\bullet-}$ radicals. At the end, the complete degradation of Methylene blue dye happens which changed into non-toxic compounds such as, SO_4^{2-}, Cl^{-1}, NO^{3-}, CO_2, H_2O, and NH_4^+ [39] (Fig. 8).

The possible mechanism of the photodegradation of the MB can be expressed as follows:

$$CuCoMn_2O_4 + h\nu \rightarrow CoMn_2O_4 + e_{cb}^- + h_{vb}^+ \quad (5)$$

$$e_{cb}^- + O_2 \rightarrow O_2^{\bullet-} \quad (6)$$

$$OH^\bullet + O_2^{\bullet-} + \text{MB dye} \rightarrow \text{Photodegradation products} \quad (7)$$

3.5.2. Photocatalytic efficiency

All above-synthesized nanoparticles were evaluated for photocatalytic activities. During the photocatalytic experiment, the efficiency of these photocatalysts was investigated by photo-aging removal of Methylene blue (MB) in visible light and monitored the decomposition rates. Photocatalyst (2 mg) was dissolved in 50 mL of 5 ppm MB dye solution and kept in dark to establish adsorption-desorption equilibria. The photocatalytic activity is

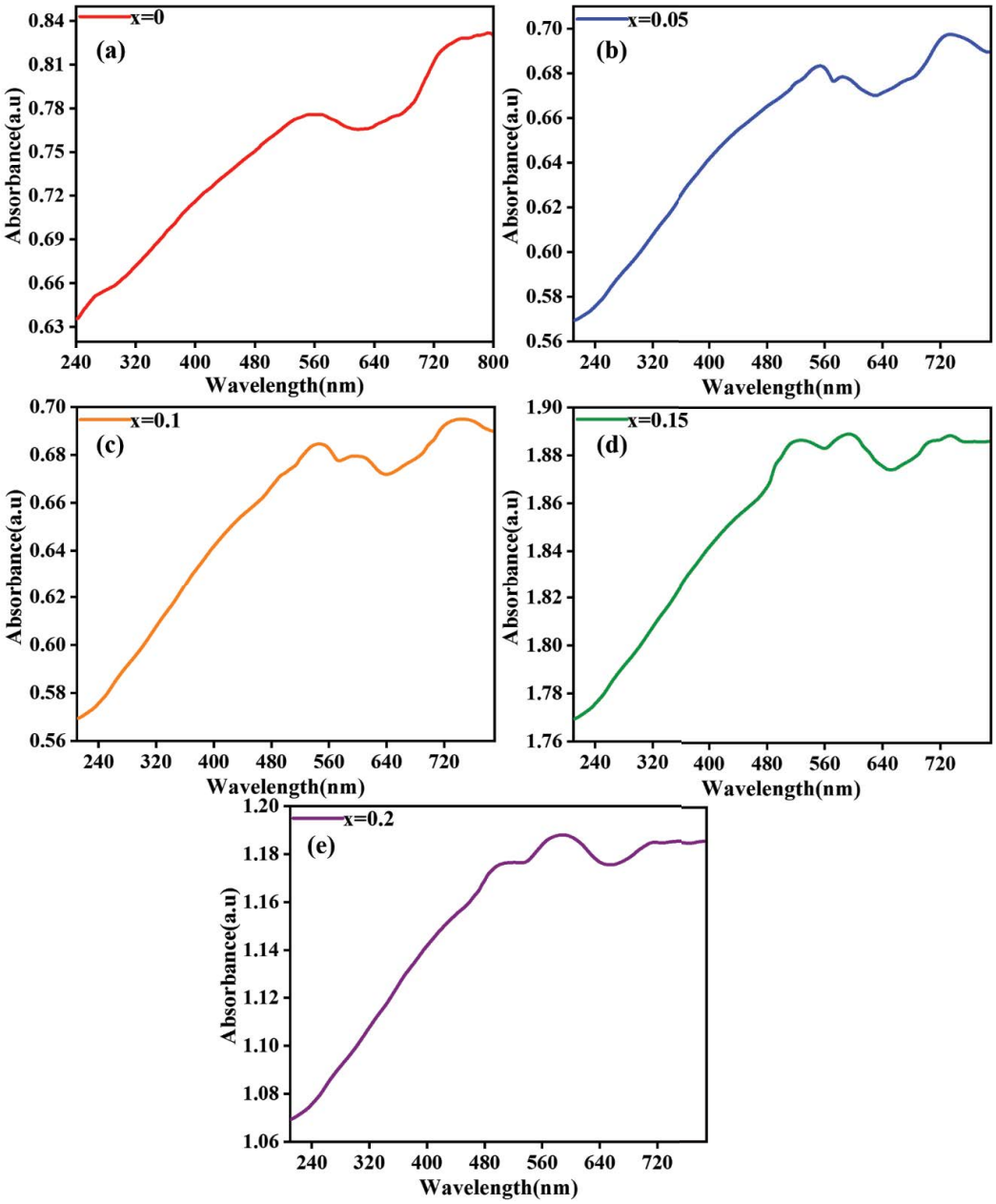

Fig. 6. UV-Vis spectrum and insect Tauc plot of (a) $Cu_0Co_{(1-0)}Mn_2O_4$ NPs, (b) $Cu_{0.05}Co_{(1-0.05)}Mn_2O_4$ NPs, (c) $Cu_{0.1}Co_{(1-0.1)}Mn_2O_4$ NPs, (d) $Cu_0Co_{(1-0)}Mn_2O_4$ NPs and (e) $Cu_{0.2}Co_{(1-0.2)}Mn_2O_4$ NPs.

gradually increased as the substituent percentage increased. After 80 min of visible light, the fall in absorption rate was seen. The degradation rate of Methylene blue (MB) in the existence of photocatalyst, commonly obeys the pseudo-first-order kinetics. The % degradation of the MB was evaluated under the given relation in Eq. (8).

$$\%\text{degradation} = \eta = \left[1 - \frac{C_0}{C_t}\right] \times 100 \tag{8}$$

where 'C_0' and 'C_t' is the concentration of dye before and after intervals of time. The value of the rate constant of the dye for the synthesized samples was measured by taking the natural logarithm of the pseudo-first-order kinetics expression in Eq. (9).

$$-\ln\left[\frac{C_0}{C_t}\right] = kt \tag{9}$$

where C_0 and C_t are the concentrations of dye before and after time intervals and k symbolized for the rate constant of pseudo-first-order [40,41]. The behavior of Cu-substituted $CoMn_2O_4$ nanoparticles towards photo-degradation is displayed in Fig. 9.

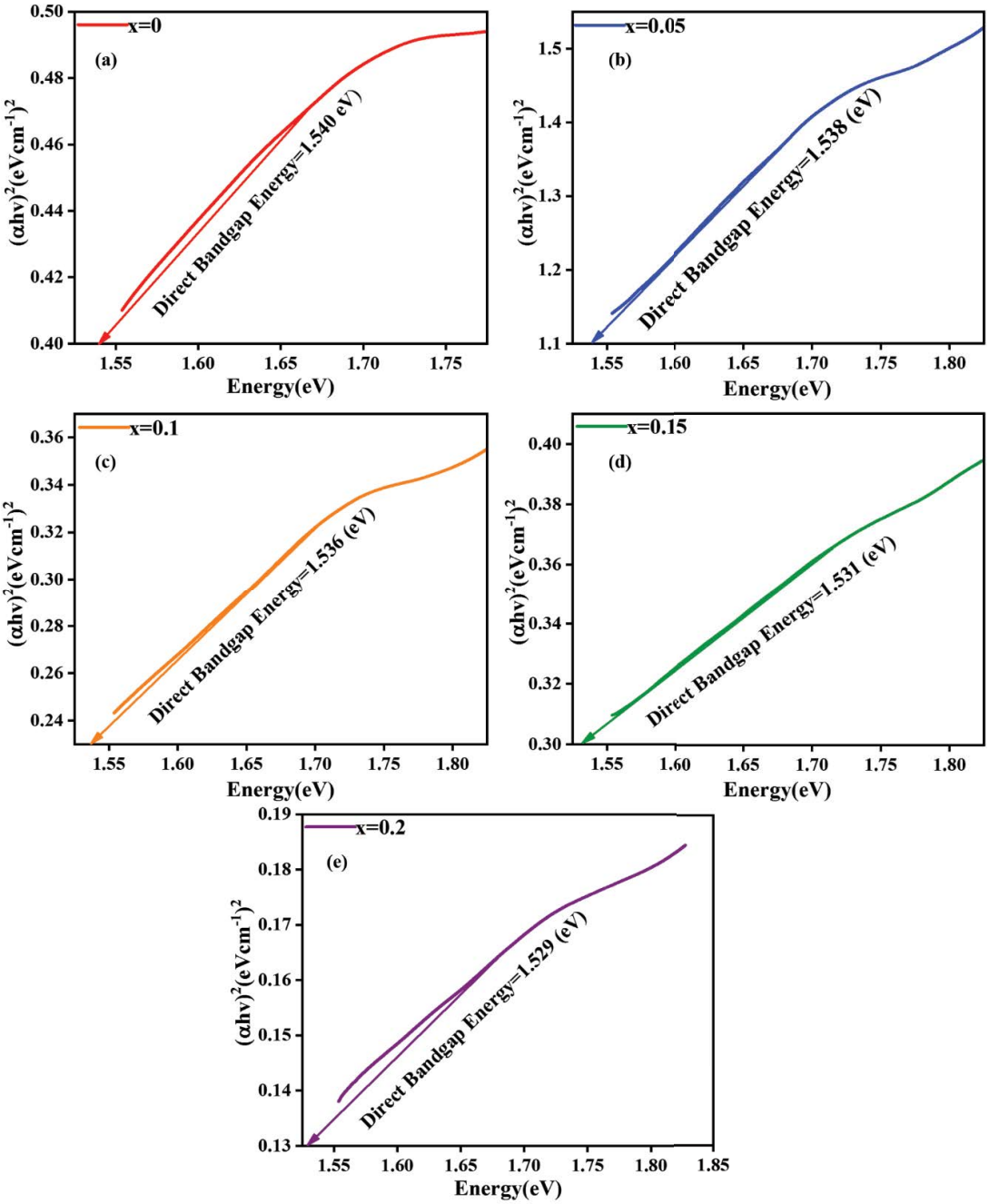

Fig. 7. Tauc plot of (a) $Cu_0Co_{(1-0)}Mn_2O_4$ NPs, (b) $Cu_{0.05}Co_{(1-0.05)}Mn_2O_4$ NPs, (c) $Cu_{0.1}Co_{(1-0.1)}Mn_2O_4$ NPs, (d) $Cu_0Co_{(1-0)}Mn_2O_4$ NPs and (e) $Cu_{0.2}Co_{(1-0.2)}Mn_2O_4$ NPs.

It was obvious from the experiment that MB dye was remained stable or slightly degraded in the absence of Cu-substituted photocatalyst under UV-Visible region. Among different nano-photocatalysts, the dye color began to fade over 30–40 min of irradiation time. After specific intervals of time, a reduction in the peak intensities of all samples was observed. After 70–80 min, complete degradation of MB dye occurred and new bands with shorter intensities were observed. The rate of degradation and kinetics of nanocatalysts of synthesized copper substituted particles are shown in Figs. 10 and 11.

When C_t/C_0 against time plotted, it was noted that the degradation of MB happened more rapidly with photocatalyst which is 20% substituted with copper than all other photocatalysts in Fig. 11.

The study of proficiency of catalysts to remove a dye, rate constant (k), and half-life ($t^{1/2}$) have been given in Table 4.

It is clearly seen (Table 4) that the degradation rate constant is increased as the percentage of the substituent of nanoparticles increased. The $Cu_{0.2}Co_{(1-0.2)}Mn_2O_4$ nanoparticle photocatalyst showed excellent results towards Methylene blue dye degradation than other Cu-substituted

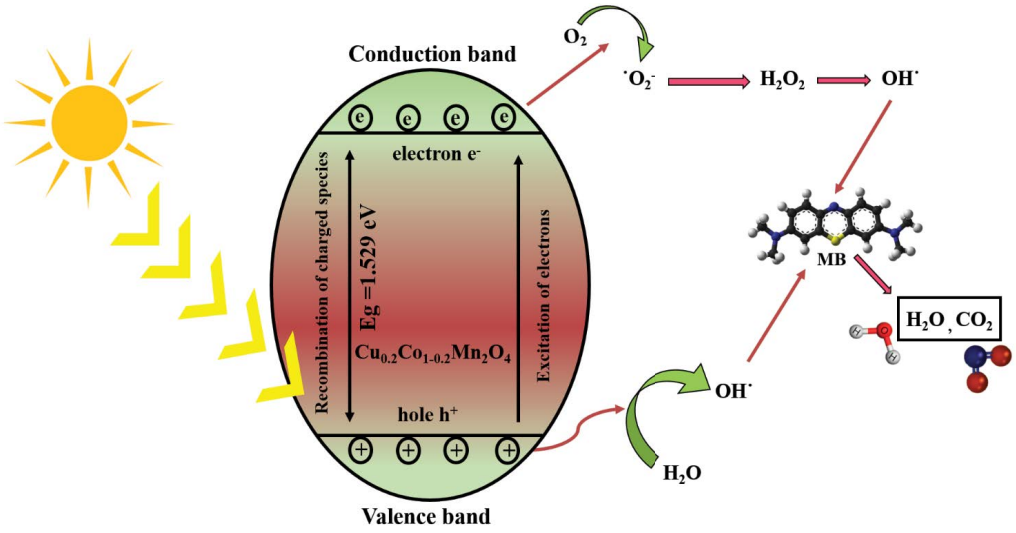

Fig. 8. The photocatalytic mechanism for $CoMn_2O_4$ photocatalyst.

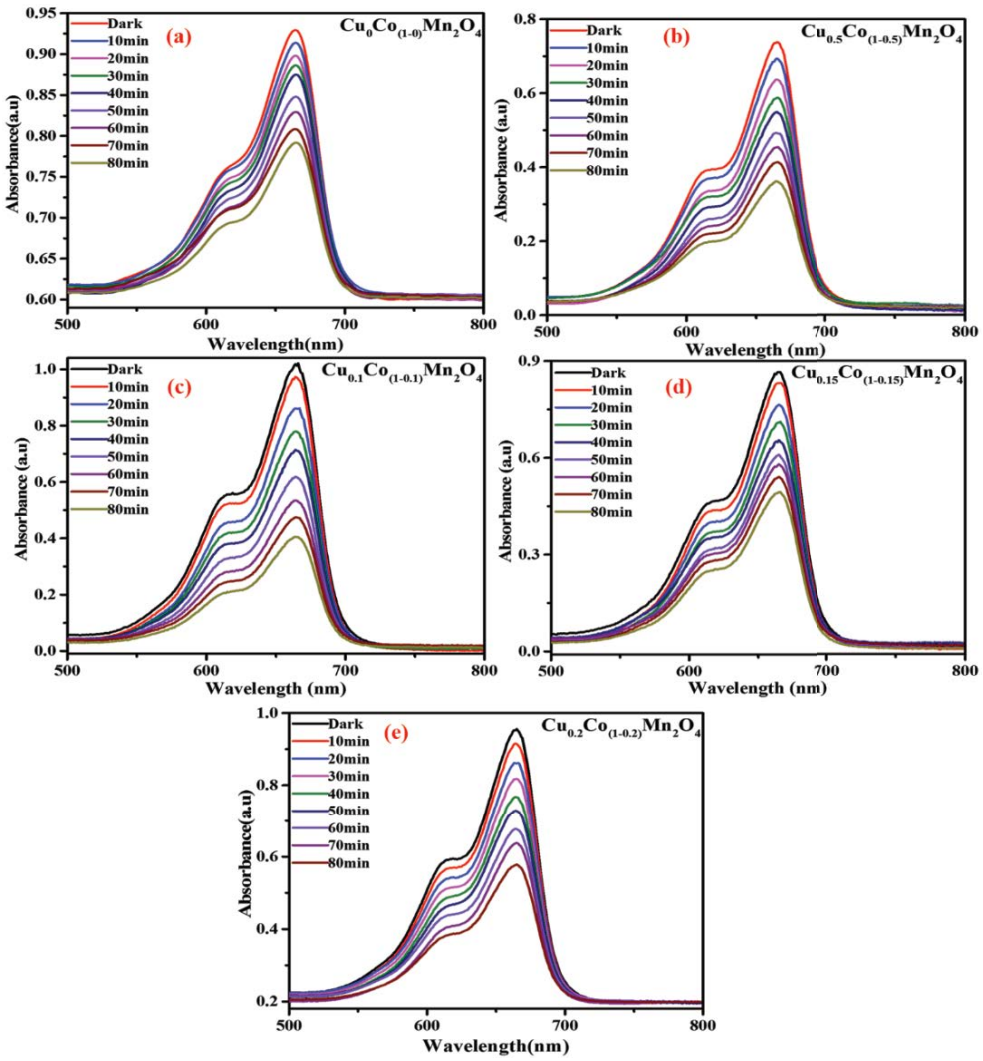

Fig. 9. Absorption spectra of MB dye solution at different time intervals in the presence of, (a) $Cu_0Co_{(1-0)}Mn_2O_4$, (b) $Cu_{0.5}Co_{(1-0.5)}Mn_2O_4$, (c) $Cu_{0.1}Co_{(1-0.1)}Mn_2O_4$, (d) $Cu_{0.15}Co_{(1-0.15)}Mn_2O_4$ and (e) $Cu_{0.2}Co_{(1-0.2)}Mn_2O_4$ NPs.

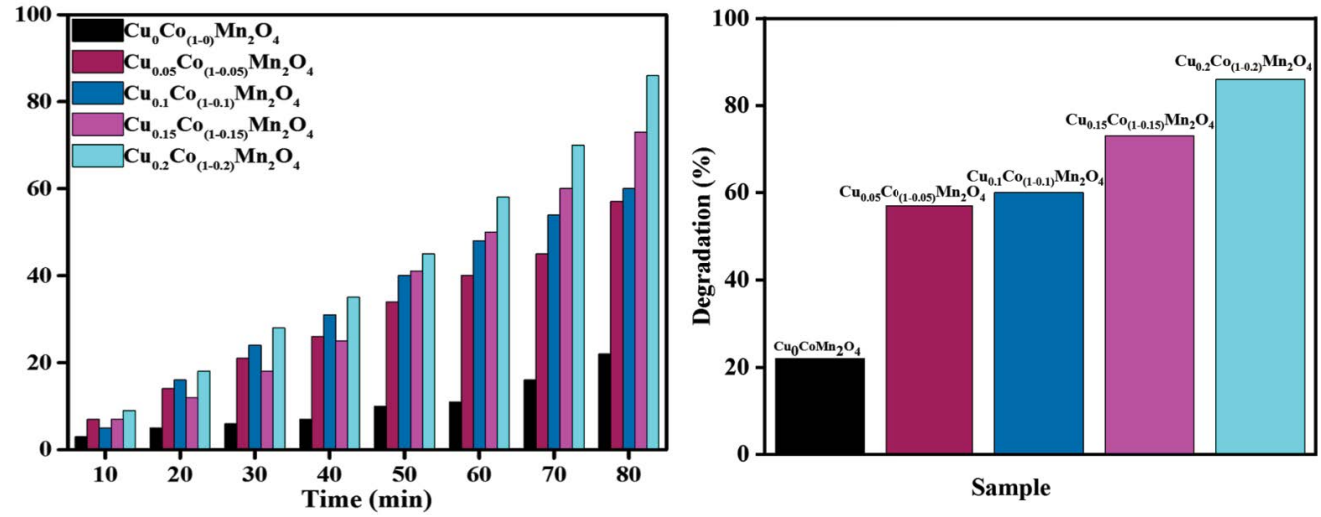

Fig. 10. % rate of degradation for MB at particular time intervals under different nano-photocatalyst.

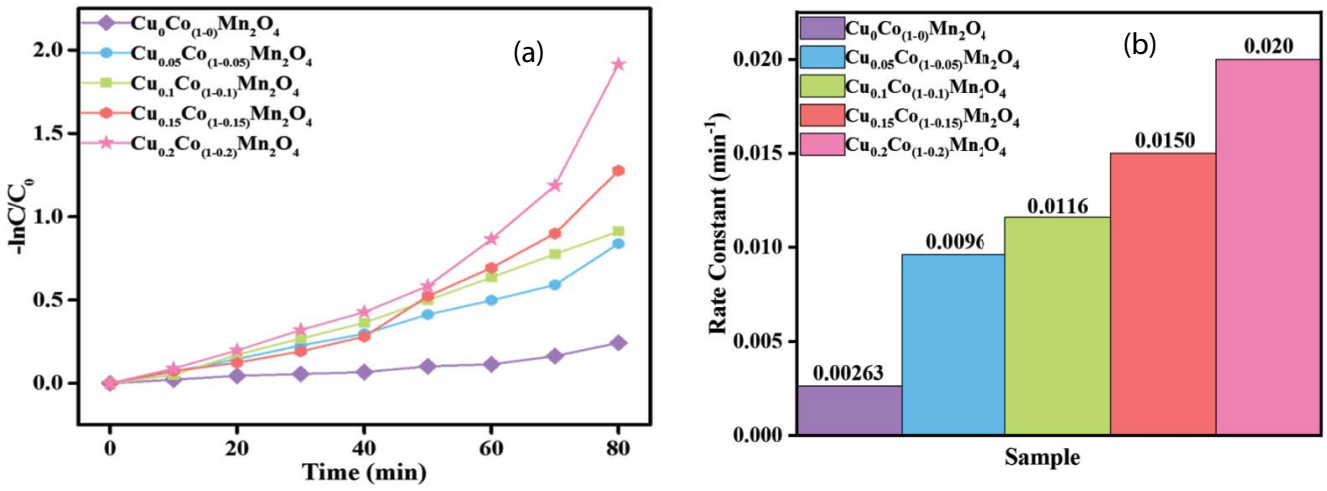

Fig. 11. Photocatalytic degradation description using UV-Vis light: (a) Kinetics of $Cu_0Co_{(1-0)}Mn_2O_4$, $Cu_{0.5}Co_{(1-0.5)}Mn_2O_4$, $Cu_{0.1}Co_{(1-0.1)}Mn_2O_4$, $Cu_{0.15}Co_{(1-0.15)}Mn_2O_4$ and $Cu_{0.2}Co_{(1-0.2)}Mn_2O_4$ NPs. (b) Comparison of rate constant of $Cu_0Co_{(1-0)}Mn_2O_4$, $Cu_{0.5}Co_{(1-0.5)}Mn_2O_4$, $Cu_{0.1}Co_{(1-0.1)}Mn_2O_4$, $Cu_{0.15}Co_{(1-0.15)}Mn_2O_4$ and $Cu_{0.2}Co_{(1-0.2)}Mn_2O_4$ NPs.

Table 4
The pseudo-first-order degradation rate (k), half-life time of reaction ($t^{1/2}$), and kinetic factors of % dye degradation for $CoMn_2O_4$ and Cu-substituted $CoMn_2O_4$ nanoparticles

Photocatalyst	Dye	% degradation	Degradation time (min)	K (min^{-1})	$t^{1/2}$
$Cu_0Co_{(1-0)}Mn_2O_4$	MB	22	80	0.00263	266.5
$Cu_{0.05}Co_{(1-0.05)}Mn_2O_4$	MB	57	80	0.0096	72.1
$Cu_{0.1}Co_{(1-0.1)}Mn_2O_4$	MB	60	80	0.0116	59.7
$Cu_{0.15}Co_{(1-0.15)}Mn_2O_4$	MB	73	80	0.0150	46.2
$Cu_{0.2}Co_{(1-0.2)}Mn_2O_4$	MB	86	80	0.020	34.6

other nanoparticles photocatalyst. Bandgap, size, and surface area of the particles are linked with heterogeneous photocatalysis. The light adsorbed by a photocatalyst is increased with an increase in surface area as a result increased in the adsorption capacity of that catalyst [42,43]. The highest photodegradation potency of $Cu_{0.2}Co_{(1-0.2)}Mn_2O_4$ is ascribed to different variables, that is, the high surface area of the materials, the tiny size of particles, short bandgap. The rate of photocatalysis is improved by providing a great number of active sites on the surface

Table 5
Comparison of present catalyst with already reported similar catalysts for degradation of various compounds

Material name	Dye	% Degradation	References
Al/Ag Co-doped MnO_2	MB	65	[44]
(n-ZnO/p-MnO) nanocomposites	Anthracene	74	[45]
Cobalt-beta hydroxyl benzoate (Co-bhb)	MB	79	[46]
$CoMn_2O_4$	MB	79.43	[47]
$Cu_{0.2}Co_{(1-0.2)}Mn_2O_4$	MB	86	Present work

of nanoparticles which can be gained by the smallest size and large surface area of the particles. Although, to elude association of photogenerated electrons and holes on the interface of the photocatalyst $Cu_{0.2}Co_{(1-0.2)}Mn_2O_4$ comparatively has a short band gap between the all five synthesized nanocatalysts and also improves the photocatalytic proficiency. This may imply that the mixture of binary metals with transition metal oxides particularly $Cu_{0.2}Co_{(1-0.2)}Mn_2O_4$ can show improved photocatalytic activity and these oxides can have a decent influence on ecological health to dissipate dangerous trashes. The comparison table of dye degradation of above-synthesized sample with other related nanoparticles are given in Table 5.

4. Conclusion

In summary, the prepared $Cu_xCo_{1-x}Mn_2O_4$ photocatalyst via co-precipitation demonstrated good photocatalytic activity for the photo-degradation of Methylene blue (MB) dye. The nanoparticles were characterized by XRD and FE-SEM and FT-IR. The result of the XRD spectra confirmed their purity. The size obtained from FE-SEM showed that the particles in nano-range. The maximum degradation was attained within 80 min. Copper substituted cobalt manganese oxide nano-photocatalyst was also used for comparative study. The $Cu_{0.2}Co_{(1-0.2)}Mn_2O_4$ showed excellent (~86%) photocatalytic performance in contrast with $Cu_0CoMn_{(1-0)}O_4$ (22%), $Cu_{0.5}Co_{(1-0.5)}Mn_2O_4$ (57), $Cu_{0.1}Co_{(1-0.1)}Mn_2O_4$ (60%), $Cu_{0.15}Co_{(1-0.15)}Mn_2O_4$ (73%) for the degradation of MB in visible light irradiation. The enhanced photocatalytic activity is mainly attributed to the development of $Cu_xCo_{1-x}Mn_2O_4$ heterojunction that not just contributed to the separation of photo-induced electron-hole pairs, but also assisted a great redox capability. Therefore, $Cu_xCo_{1-x}Mn_2O_4$ (x = 0.2) photocatalyst can be highly efficient for polluted wastewater decontamination.

Acknowledgments

Authors (Dr. Muhammad Farooq Warsi, Dr. Humera Sabeeh, and Nagina Bashir) are thankful to the Institute of Chemistry, The Islamia University of Bahawalpur (Pakistan), and Higher Education Commission (HEC-Islamabad) of Pakistan (6276/Punjab/NRPU/R&D/HEC/2016). Authors from King Saud University, sincerely appreciate the Deanship of Scientific Research, King Saud University Riyadh (Saudi Arabia) for their contribution through Research Group Project No: 1438-068. Dr. Sonia Zulfiqar is highly grateful to American University in Cairo (AUC) for financial support through the STRC mini-grant and research project No. SSE-CHEM-S.Z.-FY19-FY20-FY21-RG (1–19)-2018-Oct-01-17-53-22.

References

[1] W. Li, L. Xie, L. Zhou, J. Ochoa-Lozano, C. Li, X. Chai, A systemic study on Gd, Fe and N co-doped TiO_2 nanomaterials for enhanced photocatalytic activity under visible light irradiation, Ceram. Int., 46 (2020) 24744–24752.
[2] M. Wang, J. Ioccozia, L. Sun, C. Lin, Z. Lin, Inorganic-modified semiconductor TiO_2 nanotube arrays for photocatalysis, Energy Environ. Sci., 7 (2014) 2182–2202.
[3] J. Zheng, Y. Hu, L. Zhang, Design and construction of a bifunctional magnetically recyclable 3D $CoMn_2O_4$/CF hybrid as an adsorptive photocatalyst for the effective removal of contaminants, Phys. Chem. Chem. Phys., 19 (2017) 25044–25051.
[4] Y. Chen, Q. Lu, X. Yan, Q. Mo, Y. Chen, B. Liu, L. Teng, W. Xiao, L. Ge, Q. Wang, Enhanced photocatalytic activity of the carbon quantum dot-modified BiOI microsphere, Nano Res. Lett., 11 (2016) 60, doi: 10.1186/s11671-016-1262-7.
[5] C.-C. Nguyen, N.-N. Vu, T.-O. Do, Efficient hollow double-shell photocatalysts for the degradation of organic pollutants under visible light and in darkness, J. Mater. Chem. A, 4 (2016) 4413–4419.
[6] K. Singh, S. Arora, Removal of synthetic textile dyes from wastewaters: a critical review on present treatment technologies, Crit. Rev. Env. Sci. Technol., 41 (2011) 807–878.
[7] C.A. Martínez-Huitle, E. Brillas, Decontamination of wastewaters containing synthetic organic dyes by electrochemical methods: a general review, Appl. Catal., B, 87 (2009) 105–145.
[8] A. Bhattacharjee, M. Ahmaruzzaman, Photocatalytic-degradation and reduction of organic compounds using SnO_2 quantum dots (via a green route) under direct sunlight, RSC Adv., 5 (2015) 66122–66133.
[9] A.S. Attar, Efficient photocatalytic degradation of Methylene blue dye by SnO_2 nanotubes synthesized at different calcination temperatures, Sol. Energy Mater. Sol. Cells, 183 (2018) 16–24.
[10] P. Tan, X. Chen, L. Wu, Y.Y. Shang, W. Liu, J. Pan, X. Xiong, Hierarchical flower-like $SnSe_2$ supported Ag_3PO_4 nanoparticles: towards visible light driven photocatalyst with enhanced performance, Appl. Catal., B, 202 (2017) 326–334.
[11] F.C. Moreira, R.A.R. Boaventura, E. Brillas, V.J.P. Vilar, Electrochemical advanced oxidation processes: a review on their application to synthetic and real wastewaters, Appl. Catal., B, 202 (2017) 217–261.
[12] V. Vaiano, G. Iervolino, D. Sannino, J.J. Murcia, M.C. Hidalgo, P. Ciambelli, J.A. Navío, Photocatalytic removal of patent blue V dye on Au-TiO_2 and Pt-TiO_2 catalysts, Appl. Catal., B, 188 (2016) 134–146.
[13] M.Y. Guo, A.M.C. Ng, F. Liu, A.B. Djurišić, W.K. Chan, Photocatalytic activity of metal oxides—the role of holes and OH radicals, Appl. Catal., B, 107 (2011) 150–157.
[14] T. Kamegawa, N. Suzuki, H. Yamashita, Design of macroporous TiO_2 thin film photocatalysts with enhanced photofunctional properties, Energy Environ. Sci., 4 (2011) 1411–1416.

[15] H.E.A. Mohamed, B.T. Sone, S. Khamlich, E. Coetsee-Hugo, H.C. Swart, T. Thema, R. Sbiaa, M.S. Dhlamini, Biosynthesis of $BiVO_4$ nanorods using *Callistemon viminalis* extracts: photocatalytic degradation of Methylene blue, Mater. Today, 36 (2021) 328–335.
[16] N. Altaf, T. Anjam, M. Sajid, N. Shad, S. Shukrullah, M. Naz, Y. Javed, Characterization of manganese/cobalt oxide composites synthesized by chemical co-precipitation method, IOP Conf. Ser.: Mater. Sci. Eng., 863 (2020) 012021.
[17] X. Shi, F. Zheng, N. Yan, Q. Chen, $CoMn_2O_4$ hierarchical microspheres with high catalytic activity towards p-nitrophenol reduction, Dalton Trans., 43 (2014) 13865–13873.
[18] M.A. Salam, Synthesis and characterization of novel manganese oxide nanocorals and their application for the removal of Methylene blue from aqueous solution, Chem. Eng. J., 270 (2015) 50–57.
[19] M.Y. Nassar, S. Abdallah, Facile controllable hydrothermal route for a porous $CoMn_2O_4$ nanostructure: synthesis, characterization, and textile dye removal from aqueous media, RSC Adv., 6 (2016) 84050–84067.
[20] M. Misra, S.R. Chowdhury, N. Singh, TiO_2@Au@$CoMn_2O_4$ core–shell nanorods for photo–electrochemical and photocatalytic activity for decomposition of toxic organic compounds and photo reduction of Cr^{6+} ion, J. Alloys Compd., 824 (2020) 153861, doi: 10.1016/j.jallcom.2020.153861.
[21] A. Omidvar, B. Jaleh, M. Nasrollahzadeh, H.R. Dasmeh, Fabrication, characterization and application of GO/Fe_3O_4/Pd nanocomposite as a magnetically separable and reusable catalyst for the reduction of organic dyes, Chem. Eng. Res. Des., 121 (2017) 339–347.
[22] M. Nasrollahzadeh, M. Sajjadi, S. Iravani, R.S. Varma, Carbon-based sustainable nanomaterials for water treatment: state-of-art and future perspectives, Chemosphere, 263 (2021) 128005, doi: 10.1016/j.chemosphere.2020.128005.
[23] S. Naghdi, M. Sajjadi, M. Nasrollahzadeh, K.Y. Rhee, S.M. Sajadi, B. Jaleh, *Cuscuta reflexa* leaf extract mediated green synthesis of the Cu nanoparticles on graphene oxide/manganese dioxide nanocomposite and its catalytic activity toward reduction of nitroarenes and organic dyes, J. Taiwan Inst. Chem. Eng., 86 (2018) 158–173.
[24] M. Nasrollahzadeh, B. Jaleh, T. Baran, R.S. Varma, Efficient degradation of environmental contaminants using Pd-rGO nanocomposite as a retrievable catalyst, Clean – Technol. Environ. Policy, 22 (2020) 325–335.
[25] A. Omidvar, B. Jaleh, M. Nasrollahzadeh, Preparation of the GO/Pd nanocomposite and its application for the degradation of organic dyes in water, J. Colloid Interface Sci., 496 (2017) 44–50.
[26] M. Nasrollahzadeh, M. Sajjadi, S. Iravani, R.S. Varma, Green-synthesized nanocatalysts and nanomaterials for water treatment: current challenges and future perspectives, J. Hazard. Mater., 401 (2020) 123401, doi: 10.1016/j.jhazmat.2020.123401.
[27] M. Nasrollahzadeh, M. Sajjadi, S. Iravani, R.S. Varma, Starch, cellulose, pectin, gum, alginate, chitin and chitosan derived (nano)materials for sustainable water treatment: a review, Carbohydr. Polym., 251 (2020) 116986, doi: 10.1016/j.carbpol.2020.116986.
[28] B.F. Mohazzab, B. Jaleh, M. Nasrollahzadeh, S. Khazalpour, M. Sajjadi, R.S. Varma, Upgraded valorization of biowaste: laser-assisted synthesis of Pd/calcium lignosulfonate nanocomposite for hydrogen storage and environmental remediation, ACS Omega, 5 (2020) 5888–5899.
[29] P. Balasubramanian, T.S.T. Balamurugan, S.-M. Chen, T.-W. Chen, Simplistic synthesis of ultrafine $CoMnO_3$ nanosheets: an excellent electrocatalyst for highly sensitive detection of toxic 4-nitrophenol in environmental water samples, J. Hazard. Mater., 361 (2019) 123–133.
[30] J. Shi, K. Lei, W. Sun, F. Li, F. Cheng, J. Chen, Synthesis of size-controlled $CoMn_2O_4$ quantum dots supported on carbon nanotubes for electrocatalytic oxygen reduction/evolution, Nano Res., 10 (2017) 3836–3847.
[31] N. Bashir, M. Akhtar, H.Z.R. Nawaz, M.F. Warsi, I. Shakir, P.O. Agboola, S. Zulfiqar, A high performance electrochemical sensor for Pb^{2+} ions based on carbon nanotubes functionalized $CoMn_2O_4$ nanocomposite, ChemistrySelect, 5 (2020) 7909–7918.
[32] X. Pan, J.J. Ma, R. Yuan, X. Yang, Layered double hydroxides for preparing $CoMn_2O_4$ nanoparticles as anodes of lithium ion batteries, Mater. Chem. Phys., 194 (2017) 137–141.
[33] Z. Hu, X. Zhou, Y. Lu, R. Jv, Y. Liu, N. Li, S. Chen, $CoMn_2O_4$ doped reduced graphene oxide as an effective cathodic electrocatalyst for ORR in microbial fuel cells, Electrochim. Acta, 296 (2019) 214–223.
[34] P.K. Raul, S. Senapati, A.K. Sahoo, I.M. Umlong, R.R. Devi, A.J. Thakur, V. Veer, CuO nanorods: a potential and efficient adsorbent in water purification, RSC Adv., 4 (2014) 40580–40587.
[35] P. Vigneshwaran, M. Kandiban, S. Kumar, V. Venkatachalam, R. Jayavel, I.V. Potheher, A study on the synthesis and characterization of $CoMn_2O_4$ electrode material for supercapacitor applications, J. Mater. Sci. - Mater. Electron., 27 (2016), doi: 10.1007/s10854-016-4343-6.
[36] J. Tauc, Optical properties and electronic structure of amorphous Ge and Si, Mater. Res. Bull., 3 (1968) 37–46.
[37] Z.Y. Tian, N. Bahlawane, V. Vannier, K.K. Höinghaus, Structure sensitivity of propene oxidation over Co-Mn spinels, Proc. Combust. Inst., 34 (2013) 2261–2268.
[38] G. Wang, X. Shen, J. Horvat, B. Wang, H. Liu, D. Wexler, J. Yao, Hydrothermal synthesis and optical, magnetic, and supercapacitance properties of nanoporous cobalt oxide nanorods, J. Phys. Chem. C, 113 (2009) 4357–4361.
[39] M. Aadil, S. Zulfiqar, H. Sabeeh, M.F. Warsi, M. Shahid, I.A. Alsafari, I. Shakir, Enhanced electrochemical energy storage properties of carbon coated Co_3O_4 nanoparticles-reduced graphene oxide ternary nano-hybrids, Ceram. Int., 46 (2020) 17836–17845.
[40] J. Lin, L. Wang, Comparison between linear and non-linear forms of pseudo-first-order and pseudo-second-order adsorption kinetic models for the removal of Methylene blue by activated carbon, Front. Environ. Sci. Eng. China, 3 (2009) 320–324.
[41] F. Aisien, A. Amenaghawon, E. Ekpenisi, Photocatalytic decolourisation of industrial wastewater from a soft drink company, J. Eng. Appl. Sci., 9 (2014) 11–16.
[42] M. Shang, W. Wang, S. Sun, L. Zhou, L. Zhang, Bi_2WO_6 nanocrystals with high photocatalytic activities under visible light, J. Phys. Chem. C, 112 (2008) 10407–10411.
[43] A.T. Bell, The impact of nanoscience on heterogeneous catalysis, Science, 299 (2003) 1688–1691.
[44] M.U. Khalid, M.F. Warsi, I. Shakir, M.F.A. Aboud, M. Shahid, S.S. Shar, S. Zulfiqar, Al^{3+}/Ag^{1+} induced phase transformation of MnO_2 nanoparticles from α to β and their enhanced electrical and photocatalytic properties, Ceram. Int., 46 (2020) 9913–9923.
[45] B.L.M. Vargas, M.C. Ramirez, J.A.D. Real, J.R. López, F.J.B. Valenzuela, R.O. Borges, Y.R. Vidal, L.O. Frade, Synthesis and characterization of n-ZnO/p-MnO nanocomposites for the photocatalytic degradation of anthracene, J. Photochem. Photobiol., A, 369 (2019) 85–96.
[46] S. Sangeetha, G. Krishnamurthy, M.S. Raghavan, Electrochemical sensing and photocatalytic degradation of Methylene blue (MB) dye by cobalt-beta hydroxy benzoate complex, Mater. Sci. Semicond. Process., 101 (2019) 164–173.
[47] J.A.M. Mark, A. Venkatachalam, A. Pramothkumar, N. Senthilkumar, K. Jothivenkatachalam, J.P. Jesuraj, Investigation on structural, optical and photocatalytic activity of $CoMn_2O_4$ nanoparticles prepared via simple co-precipitation method, Physica B, 601 (2021) 412349, doi: 10.1016/j.physb.2020.412349.